

Metasurface Aided Intelligent Reflecting Surfaces for Indoor GSSK-VLC Downlink

Jifan Wu, Yanbin Zhang, Fasong Wang, Jiankang Zhang, and Zhengyu Zhu

Abstract

To provide high-quality communication in the indoor generalized space shift keying (GSSK) aided visible light communications (VLC) downlink transmission, especially when the line-of-sight (LoS) link is blocked, a metasurface aided intelligent reflecting surfaces (mIRS) scheme is proposed. By controlling the reflection characteristics of incident light in a deliberate manner provided in this paper, the proposed mIRS-assisted indoor GSSK-VLC downlink can significantly enhance the signal quality at the receiver end. Furthermore, the maximum likelihood (ML) and efficient preprocessing enabled sparsity orthogonal matching pursuit (OMP) detectors are respectively presented for the considered system. Finally, simulations are demonstrated to verify the effectiveness of the proposed mIRS-assisted indoor GSSK-VLC downlink transmission.

Index Terms

Visible light communications (VLC), generalized space shift keying (GSSK), metasurface aided intelligent reflecting surfaces (mIRS), maximum likelihood (ML), orthogonal matching pursuit (OMP)

I. INTRODUCTION

Driven by the vast increase of wireless connectivity and bandwidth-hungry applications and services, visible light communication (VLC), with its special features such as abundant

This research was supported in part by the National Natural Science Foundation of Henan Province under Grant 222102210003, in part by the National Natural Science Foundation of China under Grant 61901417 and 61901366, and in part by the National Key Research and Development Program under Grant 2019QY0302. Corresponding author: Yanbin Zhang (e-mail: ieybzhang@zzu.edu.cn).

J. Wu, Y. Zhang, F. Wang and Z. Zhu are with the School of Information Engineering, Zhengzhou University, Zhengzhou, 450001, Henan, China. (e-mails: {[ieybzhang](mailto:ieybzhang@zzu.edu.cn); [iefswang](mailto:iefswang@zzu.edu.cn); [iezyzhu](mailto:iezyzhu@zzu.edu.cn)}@zzu.edu.cn)

J. Zhang is with the Department of Computing and Informatics, Bournemouth University, Bournemouth BH12 5BB, U.K. (e-mail: jzhang3@bournemouth.ac.uk)

spectrum resources, low cost, anti-electromagnetic interference ability, high security, has been regarded as a potential alternative and complementary to radio frequency (RF) based wireless communications [1]. In indoor physical applications, if the line-of-sight (LoS) link between transmitter light-emitting diodes (LEDs) and the users' photo-detectors (PDs) is blocked, the users' communication quality will greatly degrade because of the low received power caused by diffuse reflection links [2].

Intelligent reflecting surfaces (IRS) is a planar surface consisting of an array of reflective elements, which can control the change of the phase and amplitude of the incident signal. Up to now, IRS has been widely studied in the field of RF wireless communications [3]–[5]. Within the context of unconventional RF communication paradigms, many scholars are committed to investigating how to solve communication problems and increase the quality of service [6]–[13]. One of the solutions to wireless channel fading and interference is densely deploying IRS in a wireless environment, at the same time, this scheme can further improve the channel capacity and reliability of the considered wireless communication system [6]. The spectral efficiency (SE) of IRS-assisted wireless networks has been discussed in [7]. To improve the link quality of a mobile user, an intelligent omni-surface (IOS)-assisted downlink communication system was proposed in [8] with a proper IOS phase shift design. By full-wave electromagnetic simulations, a reconfigurable metasurface with integrated reflecting and sensing capabilities was designed and investigated in [9]. Additionally, to reduce the channel training overhead and passive beamforming design complexity, in [10], a two-timescale joint active and passive beamforming scheme for an IRS-aided multi-user multi-input-single-output (MISO) system was proposed. In an IRS-aided multi-user MISO uplink wireless network with signal-to-interference-plus-noise ratio (SINR) constraints, comprehensive research on the power minimization problem was presented [11], which can work efficiently in both perfect and imperfect CSI settings. Moreover, the joint design of active-passive beamforming for IRS-aided P2P communication networks has been investigated with reflection resource management through the identification of the best-activated module subset [12]. Furthermore, the authors of [13] comprehensively summarized the applications, technical advantages, research progress, and future research directions of IRS. However, because of the different mechanisms of the transmission signals of RF and visible light, RIS-assisted approaches utilized in VLC systems are significantly different from that of the RF systems, and hence cannot be adopted directly in VLC. In this paper, we employ the metasurface-aided intelligent reflecting surfaces (mIRS) for reflection purposes in our considered indoor VLC downlink

transmission.

Spatial modulation (SM) is an attractive multiple-input multiple-output (MIMO) technology, which has been widely investigated in RF and VLC [14]. As the simplest configuration of SM, space shift keying (SSK) has a low device complexity and is easily implemented [15], it conveys information by only employing spatial symbols. Furthermore, the generalized SSK (GSSK) scheme can improve the SE obviously, which activates multiple transmitting antennas to convey information compared to the SSK scheme [16]. Aided by these results, two schemes: IRS-SSK and IRS-SM were proposed for RF communication systems in [17], and two detectors respectively termed as maximum energy-based greedy detector and maximum likelihood (ML) detector were provided.

However, the VLC scenarios cannot directly transplant the IRS-aided techniques developed for RF communications due to some factors such as average optical power constraints, peak optical power, and nonnegative constraints imposed on the visible light signals. Thus we need to investigate particular designs adapt to VLC systems. Currently, there are different considerations of IRS in VLC systems. In [18], to improve the system's performance, metasurfaces and mirror arrays were employed to intelligent reflect signals, while in [19] smart mirrors were studied to relax the LoS requirement for free-space optical (FSO) links. Additionally, the author significantly increased the directivity of the transmitting beams by proposing a simple nanoslit metasurface [20]. Furthermore, in [21], a reconfigurable beam-shaping system was proposed to permit non-line-of-sight (NLoS) FSO communications.

At the time of writing, most of the VLC systems rely on the existence of the LoS link. Therefore, in the considered indoor GSSK-VLC system, how to overcome the light-blocking problem of LoS link and the low received power characteristics of PDs in NLoS link in the service area are the key points to be considered in this paper. Although some literature considered the NLoS case, it is not specific to VLC systems. For example, an IRS array was proposed to build robust mmWave connections when the LoS link is blocked for indoor networks [22].

However, to the best of our knowledge, there is no IRS-assisted indoor GSSK-VLC downlink investigated in the literature. Hence in this paper, by the characteristics of IRS that can control the reflection characteristics of incident light deliberately, we propose an mIRS scheme for indoor GSSK-VLC downlink, which can enhance the signal quality at the receiver end. Additionally, the ML and efficient preprocessing enabled sparsity orthogonal matching pursuit (OMP) detectors are respectively presented for the considered system. The

contributions of this paper can be summarized as:

- **Novel scenario:** A novel mIRS-assisted indoor GSSK-VLC downlink scenario is proposed, as a part of next-generation indoor networks, which relies on a hybrid combination of GSSK-VLC and metasurface aided IRS. The considered system is capable of providing a high downlink throughput, while the metasurface aided IRS is capable of alleviating the LoS downlink propagation blockage problem.
- **Efficient detector:** The signal demodulation problem of this hybrid system is formulated as a sparsity reconstruction problem and evaluated by the compressed sensing (CS) theory. It is solved by an SVD preprocessing approach to make the measurement matrix satisfy the restricted isometric property (RIP) condition in CS. Enabled by SVD, an efficient iterative sparsity reconstruction OMP algorithm is proposed, which finds a near-optimal solution. By theoretical analysis, the proposed OMP detector has much lower computational complexity than the ML detector for the considered novel hybrid mIRS-assisted GSSK-VLC system.

The rest of the paper is organized as follows. The mIRS-assisted GSSK-VLC downlink system model is described in Section II. In Section III, ML and OMP detectors are proposed for the considered system. Specific parameter settings and simulation results are given in section IV. Finally, the conclusions are summarized in section V.

II. THE SYSTEM MODEL

In this paper, we consider the setup of mIRS in the context of an indoor GSSK-VLC downlink system with rectangular optical metasurface reflectors, and all reflectors placed on the wall as shown in Fig. 1. We assume that the system is equipped with N_t LEDs as the transmitter at the ceiling of the room and N_r up-facing PDs as the receiver. In indoor VLC systems, the quality of communication is closely related to the existence of LoS path, a blocked LoS path will deteriorate the communication performance greatly. Hence, we further assume that the PDs can't receive the LoS signal from the LEDs if the LoS link is blocked, however, LEDs can transmit data through the signal reflected by the IRS to the PDs. Therefore, IRS can be utilized to compensate for the LoS requirement in VLC systems. We assume that the phase-discontinuity of each IRS patch can be controlled independently. Additionally, we only consider the single reflection signal because the signal power will be greatly attenuated due to scattering after multiple reflections.

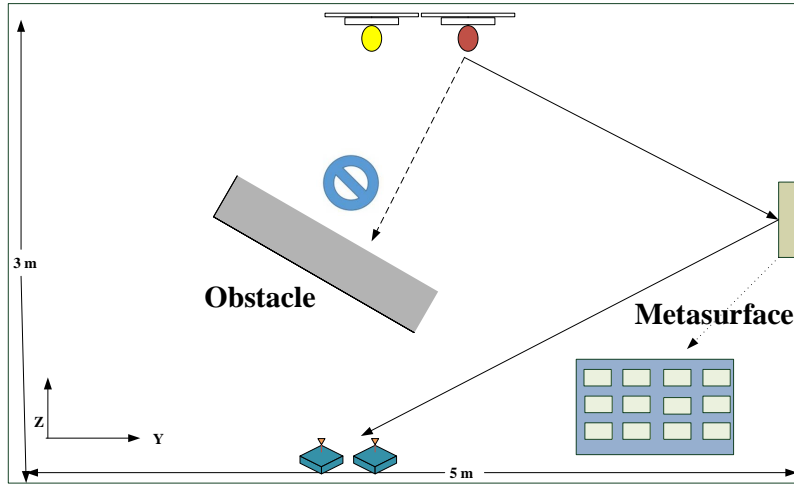


Fig. 1. IRS-assisted indoor GSSK-VLC downlink and scenarios where the LoS link is blocked.

A. Generalized Snell's law

Generalized Snell's law [18] is used to determine the direction of light rays through refractive media with varying indices of refraction, and the light reflection direction depends on the introduced phase-discontinuity in the IRS which can be adjusted by the control circuit. The reflection angle is no longer uniquely determined by the incident angle, hence the signal can be reflected in the desired direction by changing the phase-discontinuity.

Fig. 2 depicts a geometric model of an mIRS-assisted link in an indoor VLC downlink, where transmitter (LEDs) and receiver (PDs) are denoted by S and D , respectively. The reflection point of the light signal on the n -th metasurface reflector on the IRS is denoted as R_n . Suppose that the signal is reflected from point R_n on the IRS after being transmitted from S to point D , where PDs are located on the floor, which is assumed to be perpendicular to the floor and facing the ceiling. As demonstrated in Fig. 2, we define θ_n as the launch angle of LEDs, ϕ_n is the angle of incidence of PDs, θ_n^r and ϕ_n^r are incident angle and exit angle of the n -th metasurface reflector on the IRS. We assume that the reflectivity of the n -th metasurface reflector on the IRS is ρ_n . We further assume that θ_n^s represents the angle between the projection of incident light SR_n in the X-Z plane and the positive Z-axis, ϕ_n^s represents the angle between the projection of exit light R_nD in the X-Z plane and the negative Z-axis. More detailed descriptions and deviations about the mIRS-assisted VLC link can be found in [18].

In order to obtain the angles of θ_n^r , ϕ_n^r , θ_n^s and ϕ_n^s , we assume that the coordinates of S ,

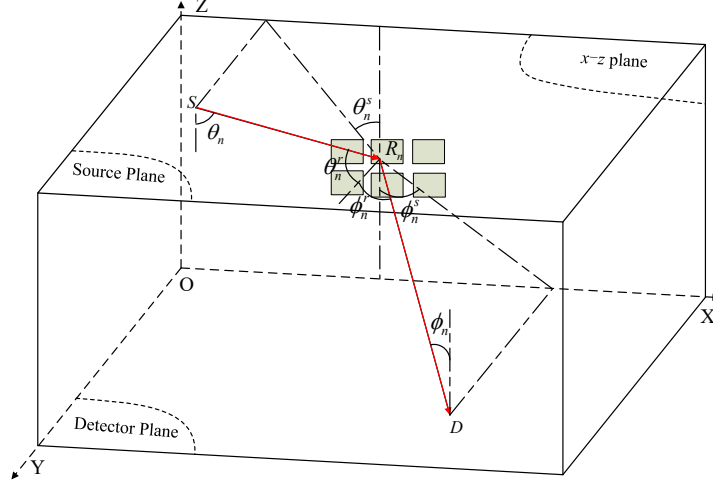


Fig. 2. Geometric model of mIRS-assisted link in indoor VLC downlink.

R_n and D are (x_1, y_1, z_1) , $(x_2, 0, z_2)$ and $(x_3, y_3, 0)$, respectively. Then, the value of these four angles can be calculated by the coordinates as follows

$$\begin{cases} \theta_n^r = \arccos\left(\frac{|y_1|}{\|\overrightarrow{SR_n}\|_2}\right), \\ \phi_n^r = \arccos\left(\frac{|y_3|}{\|\overrightarrow{R_nD}\|_2}\right), \\ \theta_n^s = \arctan\left(\frac{|x_1 - x_2|}{|z_1 - z_2|}\right), \\ \phi_n^s = \arctan\left(\frac{|x_3 - x_2|}{z_2}\right), \end{cases} \quad (1)$$

where $\|\overrightarrow{SR_n}\|_2$ and $\|\overrightarrow{R_nD}\|_2$ denotes the Euclidian distance from the transmitter to the n -th metasurface reflector on the IRS, and the n -th metasurface reflector on the IRS to the receiver, respectively. In order to direct the incident power towards the receiver detector center, the phase-discontinuity of both the X-axis and Z-axis should be calculated in three-dimensional space, which is respectively denoted as C^x and C^z . According to the results in [13], based on the derived θ_n^r , ϕ_n^r , θ_n^s and ϕ_n^s , the phase-discontinuity of the n -th metasurface reflector on the IRS C_n^x and C_n^z can be obtained by

$$C_n^x = \frac{2\pi\rho_n}{\lambda} (\sin\theta_n^r \sin\theta_n^s - \sin\phi_n^r \sin\phi_n^s), \quad (2)$$

$$C_n^z = \frac{2\pi\rho_n}{\lambda} (\sin\theta_n^r \cos\theta_n^s - \sin\phi_n^r \cos\phi_n^s). \quad (3)$$

Then, the control circuit of the mIRS can adjust the phase-discontinuity according to the results and realize the desired directional reflection of the information signals. As stated by Generalized Snell's law, it should be noted that in the reflected rays directions space, certain regions are prohibited, *i.e.*, to achieve an effective reflection, we require [21]

$$\left(\sin(\theta_n^s) \sin(\phi_n^s) - \frac{\lambda C_x^m}{2\pi \varrho_n} \right)^2 + \left(\sin(\theta_n^s) \sin(\phi_n^s) - \frac{\lambda C_z^m}{2\pi \varrho_n} \right)^2 \leq 1. \quad (4)$$

B. GSSK Modulation

GSSK enables modulation over space across different antennas at a transmitter, which can alleviate the problems such as inter-antenna interference and transmit antenna synchronization issues, it can also significantly reduce the complexity of the system while achieving an enhanced performance compared to other spatial modulation techniques [23]. In the indoor GSSK-VLC system, n_a LEDs among all N_t transmitting LEDs are activated to transmit signals, and all other LEDs are utilized for illumination. Consequently, there are $\binom{N_t}{n_a}$ possible combinations, among which $2^{\eta_{\text{GSSK}}}$ with $\eta_{\text{GSSK}} = \lfloor \log_2 \binom{N_t}{n_a} \rfloor$ are used to convey η_{GSSK} bits per symbol, and $\lfloor \cdot \rfloor$ denotes floor operation. It should be noted that SSK is a special case of GSSK modulation. For SSK, there is only one LED activated to transmit information. Therefore, the SSK transmitted information bits in each time slot is $\eta_{\text{SSK}} = \lfloor \log_2(N_t) \rfloor$. If we set $n_a = 1$, all the results derived in this paper can be applied to the SSK system [24].

Suppose that there is a GSSK scenario with $N_t = 4$ and $n_a = 2$, thus the GSSK symbol conveys $\eta_{\text{GSSK}} = 2$ bits information per symbol. For example, the mapping criterion between transmit information bits and activated LEDs combinations can be defined as: $(1, 2) \rightarrow [0, 0]$, $(1, 3) \rightarrow [1, 0]$, $(1, 4) \rightarrow [1, 1]$, $(2, 3) \rightarrow [0, 1]$, the symbol (n_i, n_j) stands for the indices of the activated LEDs, and $n_i \neq n_j$; the symbols $[m_i, m_j]$ stands for the information bits with elements $m_i, m_j = 0$ or 1 .

C. Novel mIRS-assisted indoor GSSK-VLC downlink model

In generalized Lambertian emission mode, the channel gain g between a PD and a LED through the LoS link in a conventional VLC system can be represented as [25]

$$g = \frac{(m+1)\Delta A \cos^m(\theta) \cos(\phi)}{2\pi d^2} \text{rect}\left(\frac{\phi}{\text{FOV}}\right), \quad (5)$$

where the function $\text{rect}(\cdot)$ represents that the user cannot receive the signals from LED when the field of view (FOV) of PD is smaller than the incident angle, d is the distance between

the LED and PD, ΔA represents the receiving areas of PD, m represents radiation lobe modulus, which can be calculated by

$$m = \frac{-\log(2)}{\log(\cos \Phi_{1/2})}. \quad (6)$$

$\Phi_{1/2}$ is measured from the optical axis of the LED, it represents the half irradiance at semi-angle.

In the considered indoor mIRS-assisted GSSK-VLC downlink, the channel is more complicated than the conventional GSSK-VLC system. As demonstrated in Fig. 2, the considered link can be described in two parts: 1) the channel gains from S to R_n and each reflector of the mIRS is considered as a receiver; 2) the channel gain from R_n to D and each reflector is then considered as a point source that re-emits the light signal changed by the phase-discontinuity. We further assume that d_S and d_R represent the distance from LED to IRS and IRS to PD, A_r represents the receiving areas of the reflector. Hence, the channel gain h_{ij} from j -th LED to i -th PD after reflection with N reflection elements can be approximated by a recursive algorithm as (the subscript n represents the n -th reflector of the mIRS) [26]

$$h_{ij} = \sum_{n=1}^N \frac{(m+1) \varrho_n A_r \Delta A \cos^m(\theta_n) \cos(\theta_n^r) \cos(\phi_n^r) \cos(\phi_n)}{2\pi d_{S_n}^2 d_{R_n}^2} \text{rect}\left(\frac{\phi_n}{\text{FOV}}\right). \quad (7)$$

As mentioned above, (7) is the sum of channel gains by N reflectors in the mIRS-assisted GSSK-VLC system, then the $N_r \times N_t$ channel matrix can be expressed as $\mathbf{H} = [h_{ij}]_{i=1, \dots, N_r}^{j=1, \dots, N_t}$. Finally, the received signal \mathbf{y} of the system can be expressed as

$$\mathbf{y} = \mathbf{H}\mathbf{x} + \mathbf{n}_0, \quad (8)$$

where \mathbf{y} is the N_r dimensional received signal vector by PDs, \mathbf{x} is a N_t dimensional transmission signal vector, $\mathbf{n}_0 \sim \mathcal{N}(\mathbf{0}, \sigma^2 \mathbf{I})$ is a N_r dimensional zero-mean additive white Gaussian noise (AWGN) processes received by D with variance σ^2 , and \mathbf{I} denotes an identity matrix.

III. EFFICIENT SIGNAL DETECTOR AND COMPLEXITY ANALYSIS

A. ML detector

Since the channel inputs of our considered IRS-assisted GSSK-VLC downlink system are equally likely, the optimal detector can be designed based on the ML principle [27]. As for ML optimal detector, it requires searching the active LED index one by one in the entire

search space to find the most suitable combination of active the LED index. With the highest detection accuracy, the ML detection algorithm can be formulated as

$$\hat{i} = \arg \min_{i \in \mathcal{I}} \|\mathbf{y} - \mathbf{H}_i \mathbf{x}\|^2, \quad (9)$$

where $\|\cdot\|$ denotes the Euclidean norm, \mathcal{I} indicates the set of active LEDs combinations index, \mathbf{H}_i represents the i -th channel submatrix of \mathbf{H} .

B. Sparsity aided OMP detector

Although the ML detector has the best performance, the high computational complexity makes it not practical due to exhaustive search as the number of LEDs increases dramatically. For GSSK-VLC systems with a large number of LEDs, a sparsity-aided low-complexity detection algorithm is proposed in this paper, by exploiting an efficient preprocessing procedure, it can reduce complexity significantly and achieve near-optimal bit error rate (BER) performance compared to ML detector.

As a theory of signal encoding and decoding with sparsity property, compressive sensing (CS) theory was proposed by Donoho et al. [28]. After that, a bundle of sparse signal reconstruction algorithms was provided, which includes two types of algorithms: greedy algorithm and convex optimization algorithm. The reconstruction algorithm based on convex optimization can achieve good performance, while the high computation complexity limits its practical applications. The greedy type algorithm is a suboptimal sparse reconstruction algorithm, which selects the most suitable atom and iterates continuously until it satisfies the predefined criterion. About the greedy type algorithm, OMP and a series of upgraded editions are the most popular and efficient ones [29], [30].

In CS theory, the measurement matrix \mathbf{H} should satisfy the RIP property to recover the transmitted signal \mathbf{x} accurately [28]. While as demonstrated in [25], in the proposed indoor GSSK-VLC system, it is hard to determine whether the measurement matrix satisfies the RIP property or not for the properties of channel gains. Thus, if we employ the sparse signal reconstruction algorithm to the considered system directly, the GSSK signals and the original information cannot be detected and demodulated properly. To alleviate this issue, inspired by the results in [25], the author exploited a preprocessing method of measurement matrix, and then an OMP enabled signal detector is further provided.

Motivated by [25], for the channel matrix of the considered system, in order to obey the RIP property, we explore a singular value decomposition (SVD) method to preprocess the

channel matrix (measurement matrix). Specifically, for the full row rank measurement matrix $\mathbf{H} \in \mathbb{R}^{N_r \times N_t}$, the SVD is expressed as

$$\mathbf{H} = \mathbf{W}[\mathbf{\Delta}, \mathbf{O}]\mathbf{D}^T, \quad (10)$$

where $\mathbf{W} \in \mathbb{R}^{N_r \times N_r}$ and $\mathbf{D} \in \mathbb{R}^{N_t \times N_t}$ are orthogonal matrices, $\mathbf{\Delta} = \text{diag}[\delta_1, \delta_2, \dots, \delta_{N_r}]$, and $\delta_1 \geq \delta_2 \geq \dots \geq \delta_{N_r} \geq 0$ are the singular values of \mathbf{H} , $\mathbf{O} \in \mathbb{R}^{N_r \times (N_t - N_r)}$ is a zero matrix. $(\cdot)^T$ denotes the transpose of a matrix or vector. Then, defining \mathbf{y}_{SVD} as

$$\mathbf{y}_{\text{SVD}} = \mathbf{\Delta}^{-1}\mathbf{W}^T\mathbf{y} = \mathbf{\Delta}^{-1}\mathbf{W}^T\mathbf{H}\mathbf{x} = \mathbf{F}\mathbf{x}, \quad (11)$$

where $\mathbf{F} = \mathbf{\Delta}^{-1}\mathbf{W}^T\mathbf{H}$ is the partial orthogonal matrix. Then, the preprocessed measurement matrix \mathbf{H}_{SVD} defined by \mathbf{F} can be expressed as

$$\mathbf{H}_{\text{SVD}} = \mathbf{F} \begin{bmatrix} \frac{1}{\|\mathbf{f}_1\|} & 0 & \dots & 0 \\ 0 & \frac{1}{\|\mathbf{f}_2\|} & \dots & 0 \\ \vdots & \vdots & \ddots & \vdots \\ 0 & 0 & \dots & \frac{1}{\|\mathbf{f}_{N_t}\|} \end{bmatrix} = \mathbf{F}\mathbf{\Upsilon}, \quad (12)$$

where $\mathbf{f}_1, \mathbf{f}_2, \dots, \mathbf{f}_{N_t}$ are the column vectors of the matrix \mathbf{F} , $\|\cdot\|$ is the Euclidean norm of the vector. Following this, we get

$$\mathbf{F} = \mathbf{H}_{\text{SVD}} \begin{bmatrix} \|\mathbf{f}_1\| & 0 & \dots & 0 \\ 0 & \|\mathbf{f}_2\| & \dots & 0 \\ \vdots & \vdots & \ddots & \vdots \\ 0 & 0 & \dots & \|\mathbf{f}_{N_t}\| \end{bmatrix} = \mathbf{H}_{\text{SVD}}\mathbf{\Gamma}. \quad (13)$$

Finally, the preprocessed signal can be expressed as

$$\mathbf{y}_{\text{SVD}} = \mathbf{F}\mathbf{x} = \mathbf{H}_{\text{SVD}}\mathbf{\Gamma}\mathbf{x} = \mathbf{H}_{\text{SVD}}\mathbf{x}_{\text{SVD}}, \quad (14)$$

where

$$\mathbf{x}_{\text{SVD}} = \mathbf{\Gamma}\mathbf{x}. \quad (15)$$

Consequently, the transmitted information signal can be estimated as follows after accurately reconstructing \mathbf{x}_{SVD} ,

$$\hat{\mathbf{x}} = \mathbf{\Upsilon}\mathbf{x}_{\text{SVD}}. \quad (16)$$

After this preprocessing of the measurement matrix, the classical OMP algorithm can be applied directly as proposed in Table I. In a little more detail, \mathbf{p} represents the inner product

TABLE I
OMP DETECTOR OF THE PROPOSED INDOOR MIRS-ASSISTED GSSK-VLC SYSTEM

Input:	$\mathbf{H}_{\text{SVD}}, \mathbf{y}_{\text{SVD}}, n_a$
Output:	$\hat{\mathbf{x}}, \Lambda$
1.	$\mathbf{r}_0 \leftarrow \mathbf{y}_{\text{SVD}}, t \leftarrow 0, \Lambda_0 \leftarrow \emptyset, \mathbf{A}_0 \leftarrow \emptyset$
2.	while $t \leq n_a$ do
3.	$\mathbf{p} \leftarrow \mathbf{H}_{\text{SVD}}^{\top} \mathbf{r}^{(t-1)}, \mathbb{S}_t \leftarrow \arg \max(\mathbf{p})$
4.	$\Lambda_t = \mathbb{S}_t \cup \Lambda_{t-1}, \mathbf{A}_t = \mathbf{H}_{\text{SVD}, \Lambda_t} \cup \mathbf{A}_{t-1}$
5.	$\hat{\mathbf{x}}_t = \arg \min \ \mathbf{y}_{\text{SVD}} - \mathbf{A}_t \mathbf{x}\ _2^2 = (\mathbf{A}_t^{\top} \mathbf{A}_t)^{-1} \mathbf{A}_t^{\top} \mathbf{y}_{\text{SVD}}$
6.	$\mathbf{r}_t = \mathbf{y}_{\text{SVD}} - \mathbf{A}_t \hat{\mathbf{x}}_t$
7.	end while

of the residual \mathbf{r} and the measurement matrix \mathbf{H}_{SVD} , and \mathbf{p} is calculated in each iteration. Then find the index of the maximum absolute value of \mathbf{p} and put it into the set \mathbb{S}_t . And next, we update the atomic support set matrix \mathbf{A}_t and index set Λ_t . Furthermore, $\mathbf{H}_{\text{SVD}, \Lambda_t}$ represents the submatrix of \mathbf{H}_{SVD} , and its columns are selected from the set Λ_t . Finally, the signal $\hat{\mathbf{x}}_t$ can be estimated by the least-squares method, and the residual is updated. Repeat the process until the end of the iteration of the OMP algorithm.

According to the above content, combined with SVD preprocessing and OMP algorithm, we have got the process of OMP detector, and we will perform the BER performance of this detector in the simulation section.

C. Complexity Analysis

In the proposed indoor mIRS-assisted GSSK-VLC system, both the elements of channel matrices and transmitted signals are real positive numbers. Hence, the computational complexity of the ML detector and the proposed sparsity-aided OMP signal detector are analyzed by floating-point operations (flops). Table II has shown the complexity calculation in detail.

TABLE II
COMPUTATION COMPLEXITY ANALYSIS OF THE ML DETECTOR AND THE OMP DETECTOR

Detectors	Real-valued flops
ML	$(2N_r N_t + 2N_r - 1)2^B$
OMP	$n_a N_t (2N_r - 1) + 23N_r + 5$

It should be noted that the parameter B in Table II is the spectrum efficiency in the ML

detector of the considered system. In our simulation process, the number of symbols is set to 10^5 , and the number of flops of ML is $10^5 \times (2N_r N_t + 2N_r - 1)2^B$. Consider that there is only one operation of the SVD preprocessing, and the complexity is $4N_t^2 N_r + 22N_r^3$, thus the complexity of SVD is negligible.

IV. SIMULATION AND NUMERICAL RESULTS

In this section, we suppose the service space is a $5\text{m} \times 5\text{m} \times 3\text{m}$ room, and its communication is enabled by our proposed indoor mIRS-assisted GSSK-VLC system. Two scenarios will be considered for the ML detector and OMP detector, respectively.

A. Performance analysis of the ML detector with 4 LEDs

There are two configuration schemes are considered respectively: 1) an SSK-VLC system with $N_t = 4, N_r = 2$; 2) a GSSK-VLC system with $N_t = 4, N_r = 2$ and $n_a = 2$. The LEDs are evenly arranged on the top of the room and down-facing to the floor at equal intervals. The receiver is located on the floor, which is assumed to be facing the ceiling and perpendicular to the floor. Unless specially noted, we assume that the positions of LEDs and PDs of the two configuration schemes are those presented in Table III, and the number of reflectors in the IRS is 256. The locations of one of the LED and PD are shown in Fig. 2, that is, the origin is the point O, and OX, OY, and OZ are coordinate directions. The remaining parameters are listed in Table III.

Fig. 3 depicts the BER performance comparisons of different indoor SSK and GSSK-VLC systems, which are respectively the mIRS-assisted link, conventional LoS link and diffuse reflection link. Observe from the simulation results in Fig. 3 that, if the LoS link is not blocked, the LoS link has the best BER performance. Otherwise, when the LoS link is blocked, the proposed mIRS-assisted scheme can achieve normal BER performance. When BER is 10^{-5} , the mIRS-assisted scheme has nearly 3 dB and 4.5 dB SNR performance loss of SSK and GSSK system compared with the LoS link scheme. While the diffuse reflection scheme has the worst communication performance. The reason behind this lies in that, in the diffuse reflection system with NLoS transmission, the optical path loss is more difficult to predict. It depends on multiple factors, such as room size, ceiling, wall and the reflectivity of the object, position and direction of the LEDs and PDs, window size, location and other physical factors within the room. After the light is diffusely reflected, even the strongest NLoS component is still at least 7 dB lower than the LoS component [24].

TABLE III
THE DISTRIBUTIONS OF THE LEDs' AND PDS' LOCATIONS AND SIMULATION PARAMETERS

SSK-VLC system	Coordinates
LED1	(2 m, 2 m, 3 m)
LED2	(2 m, 2.75 m, 3 m)
LED3	(2.75 m, 2 m, 3 m)
LED4	(2.75 m, 2.75 m, 3 m)
PD1	(3 m, 3.01 m, 0 m)
PD2	(3 m, 2.99 m, 0 m)
GSSK-VLC system	Coordinates
LED1	(2 m, 2 m, 3 m)
LED2	(2 m, 2.75 m, 3 m)
LED3	(2.75 m, 2 m, 3 m)
LED4	(2.75 m, 2.75 m, 3 m)
PD1	(3 m, 3.01 m, 0 m)
PD2	(3 m, 2.99 m, 0 m)
Simulation parameters	Values
IRS reflectance: ρ	0.95
IRS center position	(2.5 m, 0 m, 1.4 m)
Number of reflectors: N	256 (16×16), 64 (8×8), 16 (4×4)
Half power angle: $\Phi_{1/2}$	60°
Field of view at PD: FOV	75°
PD receiving area: ΔA	1 cm^2
Reflector area: A_r	1 cm^2
Length and width of the reflector	1 cm, 1 cm

To further explore the impact of the different number of reflectors in mIRS on the system performance, the BER performance of the proposed mIRS-assisted VLC system with 16, 64 and 256 reflectors are simulated, which are demonstrated in Fig. 4. It can be observed from Fig. 4 that the BER performance of the system is improved as the number of reflectors increases for both the SSK and GSSK-VLC systems. The main reason behind this is that the number of reflectors directly affects the receiving power at the PDs of the receiver. More precisely, as the number of metasurface reflectors increases, the receiving power of the user's receiver will enhance significantly. For practical consideration, with each reflector only occupying 1 cm^2 , an mIRS composed of hundreds or even thousands of reflectors will not occupy a lot of space.

Next, we will explore the impact of two other parameters on the BER performance of

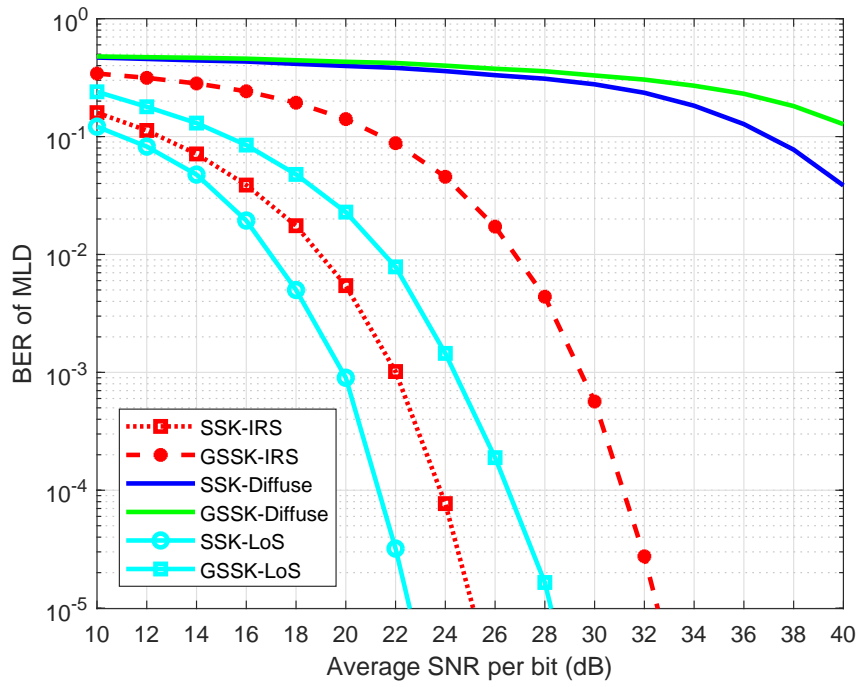


Fig. 3. BER performance comparisons of the mIRS-assisted link, conventional LoS link and diffuse reflection link of SSK and GSSK-VLC schemes based on the ML detector.

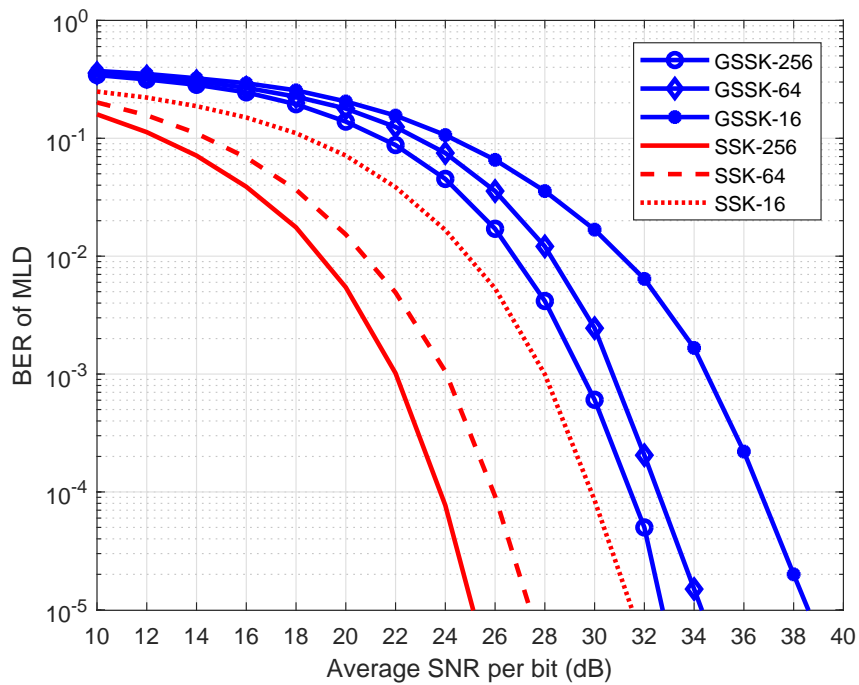


Fig. 4. The impact of different number of metasurface reflectors on BER performance with ML detector.

the proposed indoor mIRS-assisted GSSK-VLC system, which are respectively the distance between LEDs and the half-power angle of the LED. Fig. 5 demonstrates the impact of different distances between adjacent LEDs on the BER performance of the indoor mIRS-assisted VLC system for different SNRs, where the distance is set as 0.5 m, 0.75 m and 1 m, respectively, all other simulation parameters involved are the same as in Table III. Observe from Fig. 5 that the greater distance between adjacent LEDs is, the better BER performance can be gained. This is because the correlation of different channels will be decreased when increasing the adjacent LEDs distance, which will enhance the performance of the ML detection algorithm. However, it should be noted that too large spacing may lead to the marginalization of the LEDs' location in the service space and cause the transmit signal cannot be reflected by the mIRS appropriately.

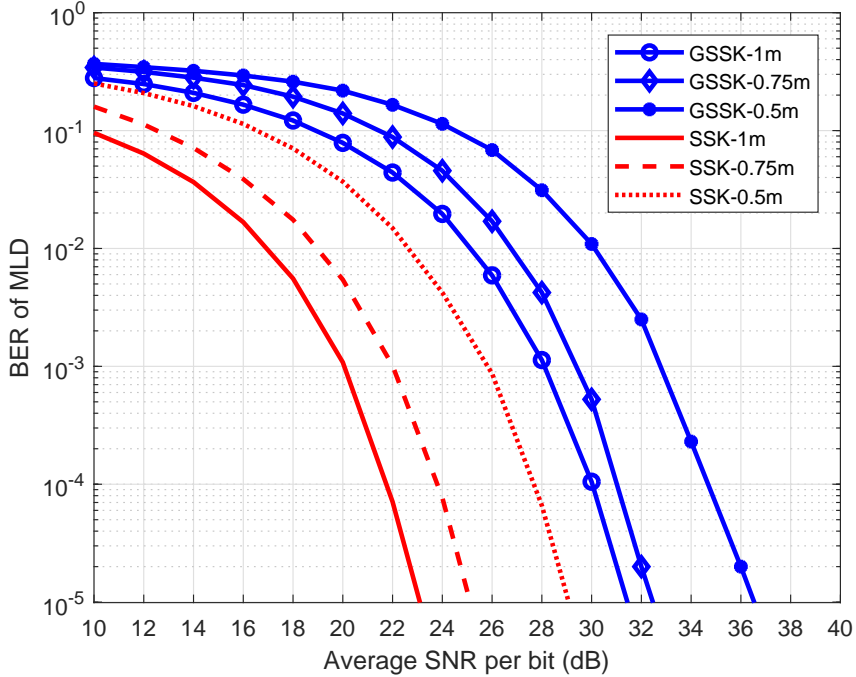


Fig. 5. The impact of different distances between adjacent LEDs on the BER performance with ML detector.

Fig. 6 characterizes the impact of different half-power angles of LED on the BER performance of the indoor mIRS-assisted GSSK-VLC system for different SNRs, where the half-power angles are set as 50° , 60° and 75° , respectively, all other simulation parameters involved are the same as in Table III. For a visible light downlink, the half-power angle mainly affects the power of the transmitted signal and the irradiation coverage of LED. Although

a smaller half-power angle can make a higher receiving power of a single beam signal, the signal cannot reach the reflectors outside the irradiation coverage of the LED. As a result obtained from Fig. 6, when the half-power angle is set as 60° , the performance can be greatly improved compared to 75° scenario. While, there is almost no reflector that can reflect the signal when the half-power angle is 50° , hence the BER performance is poor in this case.

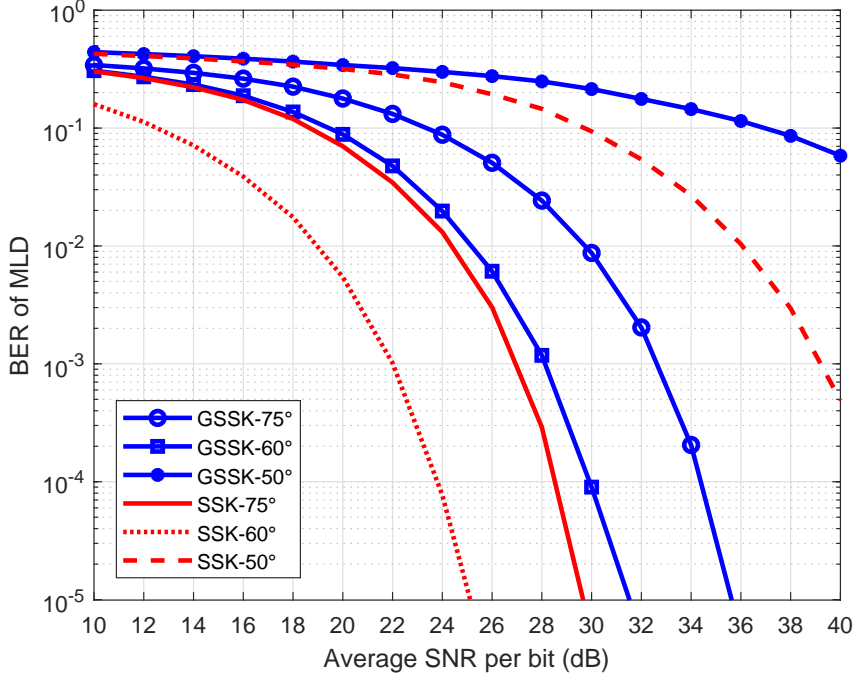


Fig. 6. The impact of different half power-angle of LED on the BER performance with ML detector.

We can learn from the above simulation that utilizing an mIRS to the indoor GSSK-VLC system can alleviate the communication problem when the LoS link is blocked. By employing this scheme, we can improve communication quality and make a better performance than diffuse reflection. Furthermore, parameters such as the number of reflectors, the distance between adjacent LEDs, and the half-power angle of LED affect the system BER performance greatly, we should carefully set these parameters in physical applications.

B. Performance analysis of the OMP detector with 9 LEDs

In this subsection, the performance of the ML detector and sparsity enabled OMP detector are considered with more LEDs and PDs than in the previous simulations. The distributions of the LEDs' and PDs' locations are provided in Table IV, and the main system simulation

parameters are the same as in the Table III. We will consider two schemes: 1) an SSK-VLC system with $N_t = 9, N_r = 4$; 2) a GSSK-VLC system with $N_t = 9, N_r = 4$ and $n_a = 2$. It should be noted that the half-power angle is set to 75° to ensure that the IRS is located within the coverage of all LEDs.

TABLE IV
THE DISTRIBUTIONS OF THE LEDs' AND PDS' LOCATIONS

9 LEDs	Coordinates
LED1	(2 m, 2 m, 3 m)
LED2	(2 m, 2.5m, 3 m)
LED3	(2 m, 3 m, 3 m)
LED4	(2.5 m, 2 m, 3 m)
LED5	(2.5 m, 2.5 m, 3 m)
LED6	(2.5 m, 3 m, 3 m)
LED7	(3 m, 2 m, 3 m)
LED8	(3 m, 2.5 m, 3 m)
LED9	(3 m, 3 m, 3 m)
4 PDs	Coordinates
PD1	(2.5 m, 2.5 m, 0 m)
PD2	(2.5 m, 2.51 m, 0 m)
PD3	(2.51 m, 2.5 m, 0 m)
PD4	(2.51 m, 2.51 m, 0 m)

Fig. 7 depicts the BER performance comparisons of the mIRS-assisted link, conventional LoS link and diffuse reflection link in indoor SSK and GSSK-VLC schemes, where the proposed OMP detector and ML detector are exploited. For the ML detector, the conventional ML and SVD aided ML are both examined. As shown in Fig. 7, the LoS link has the best BER performance by utilizing the same detector. For the proposed mIRS-assisted link, compared with the LoS link, it has nearly 6 dB and 4 dB SNR performance loss of SSK and GSSK schemes respectively when BER is 10^{-5} . As shown in Fig. 7, the diffuse reflection link has the worst BER performance. We can also infer from Fig. 7 that the proposed SVD preprocessing can significantly improve the performance of the ML detector as well. However, the ML detector has the highest computational complexity compared with the proposed OMP detector.

The impact of different half-power angles $\Phi_{1/2}$ of LED on the BER performance of the considered mIRS-assisted SSK and GSSK-VLC system versus different SNRs is shown in

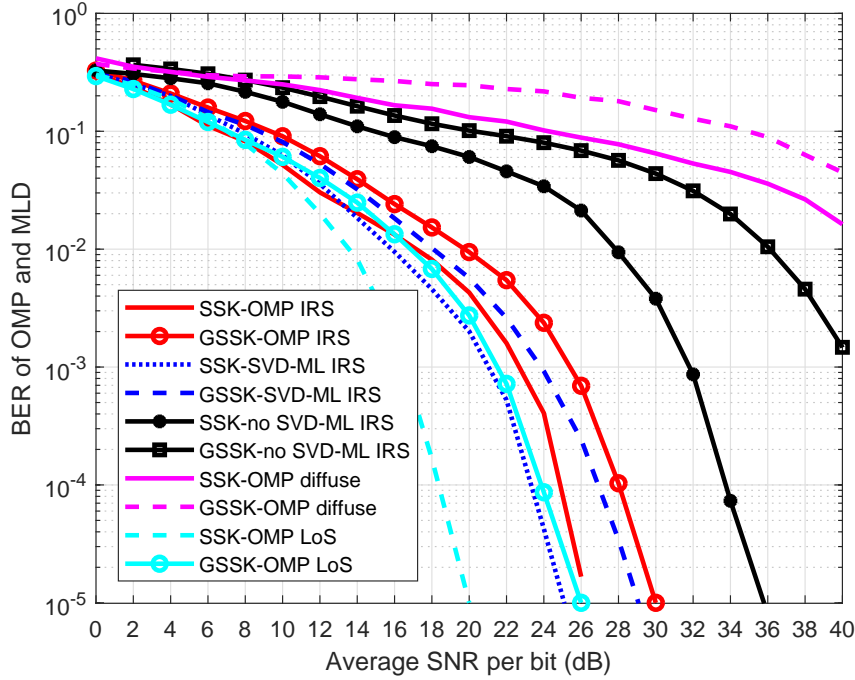


Fig. 7. BER performance of the ML detector and the OMP detector for the considered SSK and GSSK-VLC schemes, where mIRS-assisted link, conventional LoS link and diffuse reflection link are examined respectively.

Fig. 8, where the OMP detector is explored and the half-power angle $\Phi_{1/2}$ is set as 50° , 60° , 75° and 85° , respectively. All other simulation parameters involved are the same as in Table III and Table IV. As observed from Fig. 8, when the half-power angle $\Phi_{1/2}$ is 75° , the performance can be greatly improved compared to 50° and 60° scenarios. This is because, when the half-power angle $\Phi_{1/2}$ is 50° and 60° , some metasurface reflectors fail to reflect light signals and result in BER performance degradation. Especially, when the half-power angle $\Phi_{1/2}$ is 50° , there is almost no metasurface reflector that can reflect the signal from the farther LEDs. It is worth noting that due to the increase of LEDs, part of the signal cannot be reflected by the metasurface when $\Phi_{1/2}$ is set as 50° and 60° , hence a larger half-power angle $\Phi_{1/2}$ needs to be set in the case of multiple LEDs. However, as shown in Fig. 8, when we further increase the half-power angle, the BER performance will decrease to some extent. This is because a too large half-power angle is not conducive to power focusing.

Then, in order to investigate the impact of a different number of reflectors in IRS of the OMP detector performance, the BER performance of the considered system with 16, 64 and 256 reflectors are simulated respectively, which are demonstrated in Fig. 9. Observed from

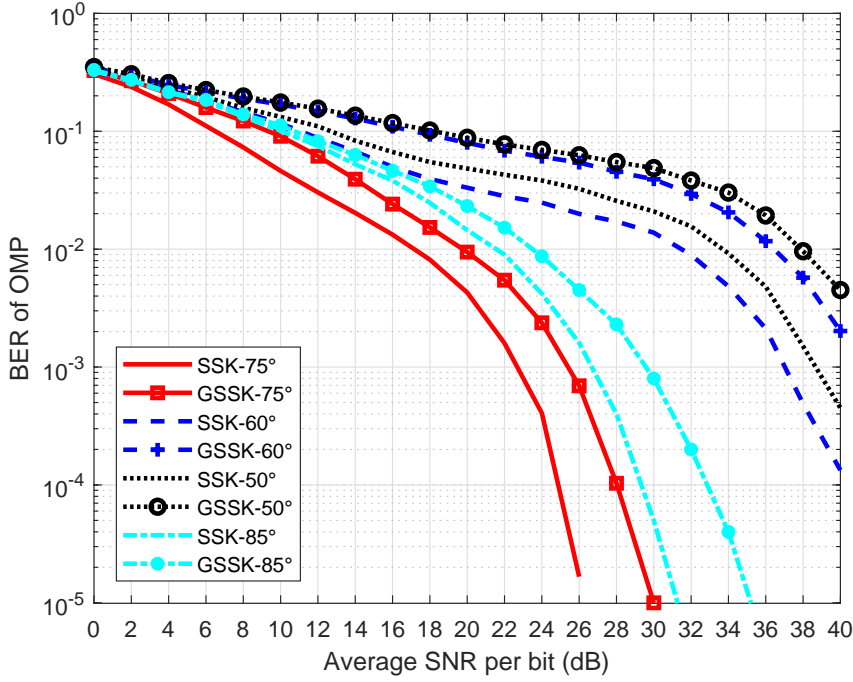


Fig. 8. The impact of different half-power angle $\Phi_{1/2}$ of LED on the BER performance of the proposed OMP detector.

Fig. 9 that the BER performance is improved as the number of reflectors increases for both the GSSK and SSK-VLC systems. The main reason behind this is that, as the number of IRS reflectors increases, the receiving power of the user's receiver PDs will enhance significantly, which is consistent with the results of the ML detector.

From the simulation results demonstrated, we can conclude that, in general, ML and OMP detectors are suitable in different scenarios for the proposed indoor mIRS-assisted GSSK-VLC system in this paper. Specifically, in a VLC system with a small number of LEDs, the ML detector is an ideal detection choice with better performance. While, when LEDs are abundant, the computation complexity of the ML detector increases sharply, and the sparsity aided OMP detector is an optimal choice.

C. Complexity Analysis

As a function of N_t and N_r when $N_a = 1$ and 2, Fig. 10 and Fig. 11 demonstrate the flops ratio of ML detector and OMP detector for SSK and GSSK systems, respectively.

We can infer from Fig.10 to Fig.11 that the ML detector has significantly higher computation complexity than the sparsity enabled OMP detector with the same system settings. This

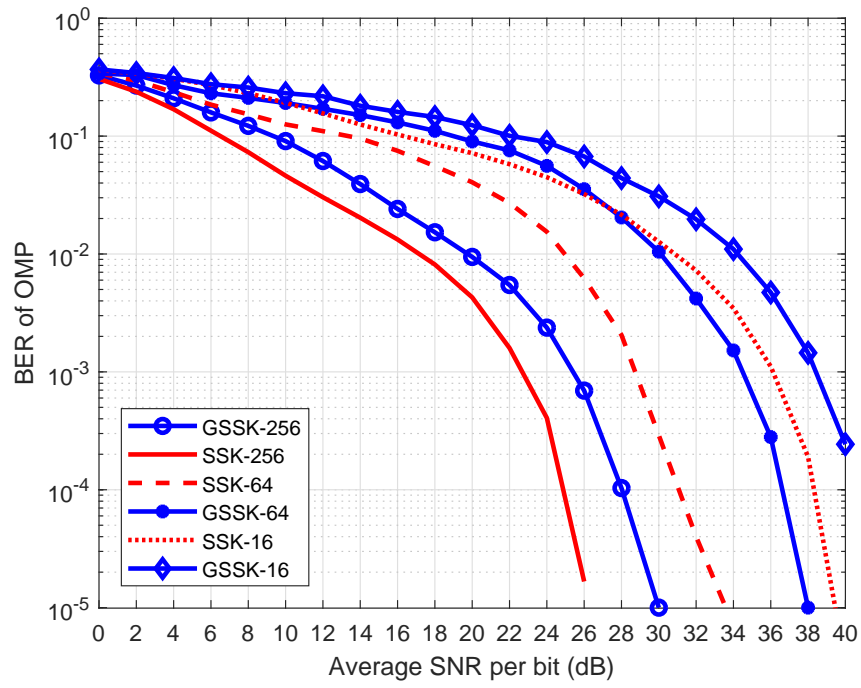


Fig. 9. The impact of the number of metasurface reflector units on BER performance of the proposed OMP detector.

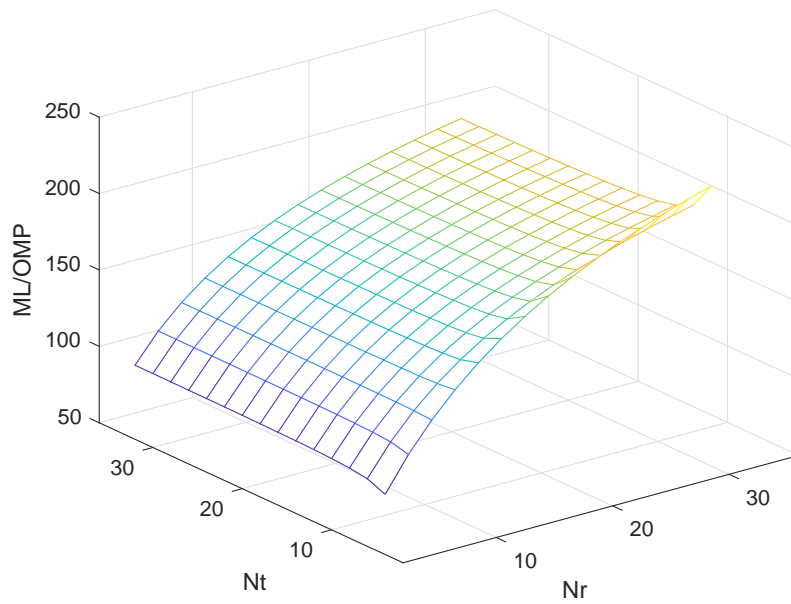


Fig. 10. The flops ratio of the ML detector and the OMP detector for indoor mIRS-assisted SSK-VLC system

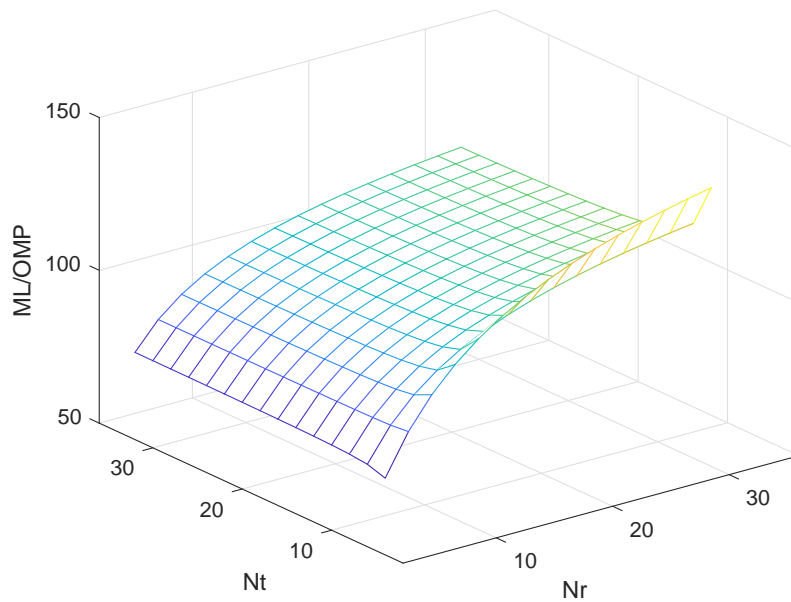


Fig. 11. The flops ratio of the ML detector and the OMP detector for indoor mIRS-assisted GSSK-VLC system

indicates that when the number of LEDs is large, the OMP detector is an ideal candidate for a MIMO VLC system.

V. CONCLUSIONS

It has been shown that IRS is particularly useful for the coverage extension and LoS blockage communication in indoor VLC systems. The mIRS-assisted indoor GSSK-VLC has been proposed in this paper as a new scheme for indoor VLC systems. Furthermore, the ML and SVD enabled OMP detectors are presented for the considered system, respectively. We have quantified the benefits of mIRS-assisted indoor GSSK-VLC through simulation results. It is found that the BER performance can be significantly improved by even a small mIRS. Furthermore, because some parameters have a relatively large impact on the performance of the considered system, some selection criteria are provided by extensive simulations. We conclude that the reasonable use of an indoor mIRS-assisted indoor GSSK-VLC scheme may be a developable paradigm.

REFERENCES

- [1] N. Chi, Y. Zhou, Y. Wei, and F. Hu, "Visible light communication in 6G: Advances, challenges, and prospects," *IEEE Vehicular Technology Magazine*, vol. 15, no. 4, pp. 93–102, 2020.

- [2] C. Valagiannopoulos, T. A. Tsiftsis, and V. Kovanis, "Metasurface-enabled interference suppression at visible-light communications," *Journal of Optics*, vol. 21, no. 11, pp. 1–8, 2019.
- [3] Q. Wu, S. Zhang, B. Zheng, C. You, and R. Zhang, "Intelligent reflecting surface-aided wireless communications: A tutorial," *IEEE Transactions on Communications*, vol. 69, no. 5, pp. 3313–3351, 2021.
- [4] Q. Wu and R. Zhang, "Towards smart and reconfigurable environment: Intelligent reflecting surface aided wireless network," *IEEE Communications Magazine*, vol. 58, no. 1, pp. 106–112, 2020.
- [5] S. Basharat, H. Pervaiz, S. A. Hassan, R. I. Ansari, H. Jung, K. Dev, and G. Huang, "Intelligent radio resource management in reconfigurable IRS-enabled noma networks," *Physical Communication*, vol. 53, p. 101744, 2022.
- [6] Z. Huang, B. Zheng, and R. Zhang, "Transforming fading channel from fast to slow: IRS-assisted high-mobility communication," in *ICC 2021 - IEEE International Conference on Communications*, 2021, pp. 1–6.
- [7] P. Nuti and B. L. Evans, "Spectral efficiency vs complexity in downlink algorithms for reconfigurable intelligent surfaces," in *2021 IEEE International Conference on Communications Workshops (ICC Workshops)*, 2021, pp. 1–7.
- [8] S. Zhang, H. Zhang, B. Di, Y. Tan, Z. Han, and L. Song, "Beyond intelligent reflecting surfaces: Reflective-transmissive metasurface aided communications for full-dimensional coverage extension," *IEEE Transactions on Vehicular Technology*, vol. 69, no. 11, pp. 13 905–13 909, 2020.
- [9] I. Alamzadeh, G. C. Alexandropoulos, N. Shlezinger, and M. F. Imani, "A reconfigurable intelligent surface with integrated sensing capability," *Scientific Reports*, vol. 11, no. 1, pp. 1–10, 2021.
- [10] M.-M. Zhao, Q. Wu, M.-J. Zhao, and R. Zhang, "Intelligent reflecting surface enhanced wireless networks: Two-timescale beamforming optimization," *IEEE Transactions on Wireless Communications*, vol. 20, no. 1, pp. 2–17, 2021.
- [11] Y. Liu, J. Zhao, M. Li, and Q. Wu, "Intelligent reflecting surface aided MISO uplink communication network: Feasibility and power minimization for perfect and imperfect CSI," *IEEE Transactions on Communications*, vol. 69, no. 3, pp. 1975–1989, 2021.
- [12] Y. Gao, C. Yong, Z. Xiong, J. Zhao, Y. Xiao, and D. Niyato, "Reflection resource management for intelligent reflecting surface aided wireless networks," *IEEE Transactions on Communications*, vol. 69, no. 10, pp. 6971–6986, 2021.
- [13] M. Di Renzo, A. Zappone, M. Debbah, M. S. Alouini, C. Yuen, J. de Rosny, and S. Tretyakov, "Smart radio environments empowered by reconfigurable intelligent surfaces: How it works, state of research, and the road ahead," *IEEE Journal on Selected Areas in Communications*, vol. 38, no. 11, pp. 2450–2525, 2020.
- [14] M. Wen, B. Zheng, K. J. Kim, M. Di Renzo, T. A. Tsiftsis, K. C. Chen, and N. Al Dhahir, "A survey on spatial modulation in emerging wireless systems: Research progresses and applications," *IEEE Journal on Selected Areas in Communications*, vol. 37, no. 9, pp. 1949–1972, 2019.
- [15] J. Jeganathan, A. Ghayeb, L. Szczecinski, and A. Ceron, "Space shift keying modulation for MIMO channels," *IEEE Transactions on Wireless Communications*, vol. 8, no. 7, pp. 3692–3703, 2009.
- [16] W. O. Popoola, E. Poves, and H. Haas, "Error performance of generalised space shift keying for indoor visible light communications," *IEEE Transactions on Communications*, vol. 61, no. 5, pp. 1968–1976, 2013.
- [17] E. Basar, "Reconfigurable intelligent surface-based index modulation: A new beyond MIMO paradigm for 6G," *IEEE Transactions on Communications*, vol. 68, no. 5, pp. 3187–3196, 2020.
- [18] A. M. Abdelhady, A. K. S. Salem, O. Amin, B. Shihada, and M. S. Alouini, "Visible light communications via intelligent reflecting surfaces: Metasurfaces vs mirror arrays," *IEEE Open Journal of the Communications Society*, vol. 2, pp. 1–20, 2021.
- [19] M. Najafi and R. Schober, "Intelligent reflecting surfaces for free space optical communications," in *2019 IEEE Global Communications Conference (GLOBECOM)*, 2019, pp. 1–7.

- [20] A. Pors, M. G. Nielsen, R. L. Eriksen, and S. I. Bozhevolnyi, "Broadband focusing flat mirrors based on plasmonic gradient metasurfaces," *Nano Letters*, vol. 13, no. 2, pp. 829–834, 2013.
- [21] Z. Cao, X. Zhang, G. Osnabrugge, J. Li, and A. Koonen, "Reconfigurable beam system for non-line-of-sight free-space optical communication," *Light Sci Appl*, vol. 8, no. 1, 2019.
- [22] X. Tan, Z. Sun, D. Koutsonikolas, and J. M. Jornet, "Enabling indoor mobile millimeter-wave networks based on smart reflect-arrays," in *IEEE INFOCOM 2018 - IEEE Conference on Computer Communications*, 2018, pp. 270–278.
- [23] Y. Sun, D. K. Borah, and E. Curry, "Optimal symbol set selection in GSSK visible light wireless communication systems," *IEEE Photonics Technology Letters*, vol. 28, no. 3, pp. 303–306, 2016.
- [24] F. Wang, C. Liu, Q. Wang, J. Zhang, R. Zhang, L. Yang, and L. Hanzo, "Optical jamming enhances the secrecy performance of the generalized space-shift-keying-aided visible-light downlink," *IEEE Transactions on Communications*, vol. 66, no. 9, pp. 4087–4102, Sep. 2018.
- [25] T. Zuo, F. Wang, and J. Zhang, "Sparsity signal detection for indoor GSSK-VLC system," *IEEE Transactions on Vehicular Technology*, vol. 17, no. 20, pp. 12 975–12 984, 2021.
- [26] Z. Ghassemlooy, W. Popoola, and S. Rajbhandari, *Optical Wireless Communications: System and Channel Modelling with MATLAB*, 1st ed. USA: CRC Press, Inc., 2012.
- [27] M. Xie, X. Yu, J. Chen, and T. Teng, "BER performance of unmanned aerial vehicle assisted spatial modulation system in rician channels," *Physical Communication*, vol. 49, p. 101471, 2021.
- [28] D. L. Donoho, "Compressed sensing," *IEEE Transactions on Information Theory*, vol. 52, no. 4, pp. 1289–1306, Apr. 2006.
- [29] J. A. Tropp and A. C. Gilbert, "Signal recovery from random measurements via orthogonal matching pursuit," *IEEE Transactions on Information Theory*, vol. 53, no. 12, pp. 4655–4666, Dec. 2007.
- [30] D. Needell and J. Tropp, "CoSaMP: Iterative signal recovery from incomplete and inaccurate samples," *Applied and Computational Harmonic Analysis*, vol. 26, no. 3, pp. 301–321, May 2009.